






Ginzburg-Landau approach to the vortex–domain wall interaction in superconductors with nematic order


R. S. Severino ^{1,2}, P. D. Mininni ^{1,3}, E. Fradkin ⁴, V. Bekeris ^{1,2}, G. Pasquini,^{1,2} and G. S. Lozano ^{1,2}

¹*Departamento de Física, Universidad de Buenos Aires, Facultad de Ciencias Exactas y Naturales, Buenos Aires 1428, Argentina*

²*CONICET–Universidad de Buenos Aires, Instituto de Física de Buenos Aires (IFIBA), Buenos Aires 1428, Argentina*

³*CONICET–Universidad de Buenos Aires, Instituto de Física Interdisciplinaria y Aplicada (INFINA), Buenos Aires 1428, Argentina*

⁴*Department of Physics and Institute for Condensed Matter Theory, University of Illinois at Urbana-Champaign, 1110 West Green Street, Urbana, Illinois 61801-3080, USA*

 (Received 16 January 2024; revised 29 February 2024; accepted 1 March 2024; published 18 March 2024)

In this work, we study the interaction between vortices and nematic domain walls within the framework of a Ginzburg-Landau approach. The free energy of the system is written in terms of a complex order parameter characteristic of *s*-wave superconductivity and a real (Ising-type) order parameter associated with nematicity. The interaction between both order parameters is described by a biquadratic and a trilinear derivative term. To study the effects of these interactions, we solve the time-dependent dissipative Ginzburg-Landau equations using a highly effective pseudospectral method by which we calculate the trajectories of a vortex that, for different coupling parameters, is either attracted or repelled by a wall, as well as of the wall dynamics. We show that despite its simplicity, this theory displays many phenomena observed experimentally in Fe-based superconductors. In particular, we find that the sign of the biquadratic term determines the attractive (pinning) or repulsive (antipinning) character of the interaction, as observed in FeSe and BaFeCoAs compounds, respectively. The trilinear term is responsible for the elliptical shape of vortex cores as well as the orientation of the axes of the ellipses and vortex trajectories with respect to the axes of the structural lattice. For the case of pinning, we show that the vortex core is well described by a heart-shaped structure in agreement with scanning tunneling microscopy experiments performed in FeSe.

DOI: [10.1103/PhysRevB.109.094513](https://doi.org/10.1103/PhysRevB.109.094513)

I. INTRODUCTION

The existence of the theoretically proposed electronic nematic phase in strongly correlated systems [1,2] has been confirmed through an amount of experimental work conducted in several systems [2]. The best documented examples of electronic nematicity are two-dimensional electron fluids in large magnetic fields at Landau levels $N \geq 1$ [3,4] and in the bilayer ruthenate $\text{Sr}_3\text{Ru}_2\text{O}_7$ (in a range of magnetic fields) [5]. Nematicity is also seen in diverse systems, and it is believed to play a central role in unconventional superconductors [6,7], in both cuprate [8–10] and iron-based [11–18] family compounds. A key fact supporting the interplay between nematic and superconducting orders is the fact that their phase boundaries, as a function of doping, intersect near the composition that maximizes the superconducting critical temperature [12], where the signature of a nematic quantum critical point has been reported [13]. A similar behavior has been reported recently in the family of nickel compounds $\text{Ba}_{1-x}\text{Sr}_x\text{Ni}_2\text{As}_2$ [19,20].

Electronic nematic order [2] is a state of the electronic fluid that *spontaneously* breaks the point group symmetry of the underlying lattice. In this paper, we will consider the case of systems with translational symmetry along the *c* axis and native C_4 point group symmetry of the *a*-*b* plane spontaneously broken down to one of its C_2 subgroups, with symmetry $d_{x^2-y^2}$ or d_{xy} . Although this is the most common case, other point group symmetries, such as C_6 , are relevant in several systems such as dichalcogenide [21] and kagome materials [22].

Several microscopic mechanisms can give rise to an electronic nematic state including a Pomeranchuk instability [23–25], orbital order [26,27], or they can arise as a vestigial order of a magnetically [28,29] and/or charge-ordered state [30,31]. Electronic nematic states typically do not arise in weakly interacting systems and are the result of strong correlation effects.

In most experimental situations, the nematic phase manifests as the result of the breaking of a *discrete* C_4 point-group symmetry of the underlying crystal structure of the material. It is generally expected that in a nematic state, the crystal should distort since there is always a coupling between the electronic degrees of freedom and the lattice. How large this distortion is depends on the microscopic mechanism behind the nematic order. In some systems, such as in the underdoped $\text{YBa}_2\text{Cu}_3\text{O}_{7-\delta}$, the orthorhombic crystal structure sets in at high temperatures, and electron nematicity is observed as an ordering effect seen at lower temperatures [9]. On the other hand, in some pnictides, such as in $\text{Ba}(\text{Fe}_{1-x}\text{Co}_x)_2\text{As}_2$, nematic order (without long-range magnetic order) arises on a relatively small fraction of the phase diagram, while in FeSe this situation occurs in a broader range of temperatures and doping.

We should note that it is conceptually important to distinguish a tetragonal-to-orthorhombic structural transition from an electronic nematic transition even though both break the same point group symmetry. Most structural transitions are typically first-order phase transitions and generally do

not exhibit significant thermal ordering effects. In contrast, electronic nematic transitions can be continuous and have significant thermal fluctuations near the ordering transition. The nematic transition in the Fe superconductors appears to be either continuous or weakly first order, which strongly suggests that it is primarily driven by an electronic mechanism. The Curie law divergence of the nematic susceptibility in the tetragonal phase is another piece of evidence supporting its electronic origin [13,32]. However, since the nematic state breaks the same symmetries as an orthorhombic crystal structure, it is hard to disentangle both effects. In particular, many experiments often show a concurrent breaking of the C_4 symmetry in the structural and transport properties consistent with a transition driven by electronic degrees of freedom [14–18]. On the other hand, despite the considerable amount of experimental evidence of the existence of electronic nematicity in Fe superconductors, there is still no consensus on its microscopic origin.

One of the consequences of the appearance of a symmetry-breaking nematic phase is the formation of a dense array of structural and nematic domains (ND), which has been observed and characterized by several techniques [12,33]. The role of these domains and the walls separating them, the so-called nematic domain walls (NDW), in the properties of the normal metallic phase is still under intense study and debate [34,35].

An interesting and less explored issue concerns the relevance of the nematic domains in the superconducting phase. For instance NDW will, in principle, interact with superconducting vortices. As nematicity is naturally coupled to anisotropic strain, the existence of nematic domains has been linked in some systems to the existence and location of *structural twin boundaries* (TB), which have been identified in several works as sources of correlated vortex pinning (and in some cases of vortex channels) on their own [36–39]. The influence of NDW/TB in the vortex dynamics in Fe-based nematic superconductors has been reported in different magnetic and transport experiments [12,40,41], and the NDW/TB-vortex interaction has been directly observed in FeSe [42–45] and $\text{Ba}(\text{Fe}_{1-x}\text{Co}_x)_2\text{As}_2$ [46–48] compounds. While in the first case vortices are pinned by domain boundaries, in the second case vortices avoid them.

At a phenomenological level, the interplay between nematicity and superconductivity can be described in principle via the Ginzburg-Landau (GL) formalism. In its simpler version, the GL free energy can be expressed as a functional of two order parameters, a complex field associated with superconductivity and a real (Ising-type) field associated with nematicity. To lowest order, these fields are coupled via a trilinear term (involving derivatives) and a biquadratic term. The main effect of the trilinear term is to give rise to an anisotropy in the superfluid density of the superconducting state, and it manifests in the elliptical shape of vortex cores. Although the coefficient of the biquadratic term has to satisfy certain bounds, its sign is not fixed *a priori*, representing order competition (cooperation) when it is positive (negative). Experimentally, the cooperative or competitive coupling manifests in several ways. For example, in-plane anisotropic superconducting properties are reflected in elongated superconducting vortices oriented along the crystallographic axes

of the orthorhombic phase, as observed in early scanning tunneling microscopy (STM) studies in FeSe superconductors [42]. Also, flux flow resistivity anisotropy [41], anisotropic critical current density [49], and an anisotropic superconducting gap [50] are additional evidence for in-plane broken symmetry in the superconducting properties.

Finally, it is worth mentioning that the coupling of electronic nematicity with strain might be more complex than generally believed [51]. However, even in a simpler scenario in which NDW are univocally linked with structural TB, they are an *additional* source of pinning (or antipinning) in such a way that the final vortex–domain wall interaction will result from the combination of structural and nematic vortex interactions.

The purpose of this work is to analyze from a theoretical perspective some properties of the NDW-vortex interaction in the framework of a time-dependent GL theory. To this end, we will use the simplest GL theory of a nematic superconductor, with an *s*-wave superconductor order parameter and an Ising-like nematic order parameter. Nematic domain walls can be present for two types of nematic orders with d_{xy} and $d_{x^2-y^2}$ symmetry, respectively, and the elliptically distorted vortices are oriented differently relative to the crystallographic axis. For definiteness, in the body of the paper we consider primarily the d_{xy} nematic ordering. To further characterize the interaction, we calculate trajectories, energies, and forces as a function of time and distance. Despite the simplicity of the model, we find that many features are qualitatively consistent with experimental findings. The model can successfully capture the elongation of vortex cores in the presence of nematic ordering, and it reproduces the pinning (antipinning) of vortices on domain walls as well as other features observed in experiments.

This paper is organized as follows. In Sec. II we describe the phenomenological GL model for the coupled superconducting and scalar nematic order parameters. The main calculations are presented in Sec. III organized in different subsections. The numerical method is described first, followed by the domain boundary effect in the superconducting order parameter and in the single vortex dynamics, where the role of the biquadratic and trilinear coupling terms is considered. Finally, a summary and conclusions are presented in Sec. IV.

II. GINZBURG-LANDAU MODEL

The total Ginzburg-Landau (GL) free energy of interest is

$$F = F_S + F_N + F_{SN}, \quad (1)$$

where F_S is the standard energy for an *s*-wave complex superconductor order parameter ψ , F_N is the free energy for a real Ising-type nematic order parameter, and F_{SN} is the coupling energy between them. For F_S we write

$$F_S = \int_V \left[\alpha_{\text{GL}} |\psi|^2 + \frac{\beta}{2} |\psi|^4 + \frac{\hbar^2}{2m} |\mathcal{D}\psi|^2 + \frac{(\nabla \times \mathbf{A})^2}{8\pi} \right], \quad (2)$$

where the superfluid Cooper pair density is $n_s = |\psi|^2$, \mathbf{A} is the magnetic vector potential that relates to the magnetic induction as $\nabla \times \mathbf{A} = \mathbf{B}$, and $\mathcal{D} = -i\nabla - \frac{e}{\hbar c} \mathbf{A}$ is the covariant derivative. Although m stands for a parameter with dimen-

sions of mass, it should not be taken as the mass of any particle or quasiparticle but as a parameter related to the phase stiffness of the order parameter. The charge of the Cooper pairs (twice the electron charge) will be denoted as e , while \hbar and c are the reduced Planck constant and the speed of light, respectively.

We will consider configurations that are translational invariant along the c -direction, which implies that any dependence on this coordinate will hereby be ignored. As for the coordinates in the ab plane, attention has to be drawn to the choice of axes. In Fe-based superconductors (as well as in many cuprates), nematicity occurs simultaneously with a tetragonal to orthorhombic structural phase transition, with the ab basis rotated in a $\pi/4$ angle between the different phases. In this work, we will choose our ab base to coincide with that of the tetragonal phase.

The contribution of the nematic Ising-type order parameter to the GL free energy is given by

$$F_N = \int_V \left[\gamma_2 (\nabla \eta)^2 + \gamma_3 \eta^2 + \frac{\gamma_4}{2} \eta^4 \right], \quad (3)$$

while the coupling between superconductivity and nematicity is given by two terms,

$$F_{SN} = F_{bi} + F_{tr}. \quad (4)$$

The first one is a biquadratic coupling of the form

$$F_{bi} = \lambda_2 \int_V \eta^2 |\psi|^2. \quad (5)$$

This term indeed does not depend on the specific character of the nematic order parameter, and it could be present even if η was a true scalar field.

In addition, there could be a trilinear term of the form

$$F_{tr} = \frac{\hbar^2}{2m} \lambda_1 \int_V \eta e_{ij} \mathcal{D}_i \psi (\mathcal{D}_j \psi)^*, \quad (6)$$

where

$$e_{ij} = 2(n_i n_j - \frac{1}{2} \delta_{ij}), \quad (7)$$

and $\mathbf{n} = (\cos \alpha, \sin \alpha)$ is the director signaling orientation of the nematic order with respect to the coordinate basis (which in this work corresponds to the tetragonal phase). A model of this type was used, for instance, in [52] to study vortices in the London limit, and more recently in [53] where vortex-vortex interactions were analyzed.

In the present paper, and inspired by nematicity in Fe-based superconductors, we will choose α as follows: As the director aligns according to one of the orthorhombic axes, if we choose \hat{x} and \hat{y} directions to coincide with the tetragonal axis, then $\alpha = \pi/4$ (cf. [52,53], where \hat{x} and \hat{y} were chosen as the orthorhombic axis and then $\alpha = 0$). During the phase transition, structural domains with different orientations of the orthorhombic axes can form, separated by a domain wall or twin boundary as shown schematically in Fig. 1(a).

Note that while the biquadratic coupling between the nematic and superconductor order parameters can be present even in the case in which η is a standard scalar field, the trilinear term is instead a genuine nematic coupling. The biquadratic coupling parameter λ_2 can be either positive or

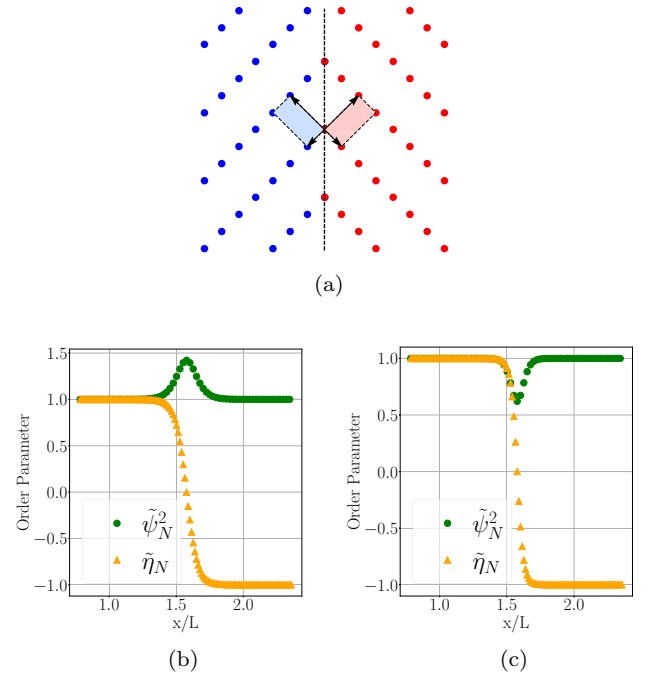


FIG. 1. (a) Schematic representation of the domain wall and the broken orthorhombic symmetry. Notice that the crystalline orthorhombic axes at each side of the wall form a 45° angle with the wall. (b) Profile of the normalized superconductor $\tilde{\psi}_N^2 = \frac{|\psi|^2}{\psi_0^2}$ and nematic $\tilde{\eta}_N = \frac{\tilde{\eta}}{\tilde{\eta}_0}$ [see Eqs. (10) and (16) for definitions] order parameters for the competing case with $\hat{\lambda}_2 > 0$. (c) Same as (b) but for the cooperative case with $\hat{\lambda}_2 < 0$.

negative (within some bounds), resulting in competition or cooperation of the nematic order parameter with superconductivity. A nonzero λ_1 , on the other hand, will result in elliptical vortices and its sign will select the orientation of the major axis of the ellipse with respect to the nematic order director.

As we did in [53], we consider dissipative dynamics [54] and write the time-dependent equations for the order parameters and the electromagnetic fields as

$$\frac{\hbar^2}{2mD} \partial_t \psi = -\frac{\delta F}{\delta \psi^*}, \quad \frac{\sigma}{c^2} \partial_t \mathbf{A} = -\frac{\delta F}{\delta \mathbf{A}}, \quad \frac{\hbar^2}{2mD_n} \partial_t \eta = -\frac{\delta F}{\delta \eta}. \quad (8)$$

In the above expressions, D and D_n are two diffusion constants (one for each order parameter, and not necessarily equal), and σ is the electrical conductivity of the normal state.

Three different length scales are present in the system, namely

$$\xi^2 = \frac{\hbar^2}{2m|\alpha_{GL}|}, \quad \lambda_L^2 = \frac{mc^2}{4\pi e^2 \rho_0}, \quad l_\eta^2 = \frac{\gamma_2}{|\gamma_3|}, \quad (9)$$

where ξ , λ_L , and l_η are the bare superconductor coherence length, the bare London penetration length (where $\rho_0 = \frac{|\alpha_{GL}|}{\beta_{GL}}$), and the bare nematic coherence length, respectively. We can rewrite the superconductor and nematic order parameters in terms of two dimensionless order parameters $\tilde{\psi}$ and $\tilde{\eta}$ as

$$\psi = \sqrt{\rho_0} \tilde{\psi}, \quad \eta = \eta_0 \tilde{\eta}, \quad (10)$$

where $\eta_0^2 = \frac{|\gamma_3|}{\gamma_4}$, and redefine the vector potential in terms of a simpler quantity \mathbf{a} as

$$\mathbf{A} = \frac{mc|\alpha_{\text{GL}}|}{\hbar e} \mathbf{a}. \quad (11)$$

In terms of the newly defined variables, the total free energy can be written as

$$\begin{aligned} F = & |\alpha_{\text{GL}}| \rho_0 \int_V \frac{1}{2} (|\tilde{\psi}|^2 - 1)^2 + \xi^2 |\nabla \tilde{\psi}|^2 - \mathbf{a} \operatorname{Im}(\tilde{\psi}^* \nabla \tilde{\psi}) \\ & + \frac{1}{4\xi^2} \mathbf{a}^2 \tilde{\psi}^2 + \frac{\kappa^2}{4} (\nabla \times \mathbf{a})^2 + \Gamma_2 (\nabla \tilde{\eta})^2 + \frac{\Gamma_4}{2} (\tilde{\eta}^2 - 1)^2 \\ & + \hat{\lambda}_2 \tilde{\eta}^2 \tilde{\psi}^2 - \xi^2 \hat{\lambda}_1 \tilde{\eta} [(\mathcal{D}_x \psi)^* \mathcal{D}_y \psi + (\mathcal{D}_y \tilde{\psi})^* \mathcal{D}_x \tilde{\psi}], \quad (12) \end{aligned}$$

where, as we mentioned before, we have set the director angle for the nematic parameter as $\alpha = \pi/4$, and we have redefined the parameters as

$$\begin{aligned} \Gamma_2 &= \frac{\gamma_2}{|\alpha_{\text{GL}}|(\rho_0/\eta_0^2)}, & \Gamma_4 &= \frac{\gamma_4 \eta_0^2}{|\alpha_{\text{GL}}|(\rho_0/\eta_0^2)}, \\ \hat{\lambda}_2 &= \frac{\lambda_2 \eta_0^2}{|\alpha_{\text{GL}}|}, & \hat{\lambda}_1 &= \frac{\lambda_1 \eta_0}{\hbar}. \quad (13) \end{aligned}$$

We have also introduced the GL parameter in its usual definition as

$$\kappa = \frac{\lambda_L}{\xi}. \quad (14)$$

The GL parameter is dimensionless and expresses the ratio between two characteristic lengths. In standard s -wave superconductors without nematicity, a condition of $\kappa > 1/\sqrt{2}$ is necessary for type II superconductivity. For nematic superconductors this condition has been revisited in [53]. In many realistic superconductors, the London penetration depth λ is much greater than the coherence length ξ , allowing κ to easily be higher than 100. However, for certain Fe-based materials, reported values for κ are on the order of 20 [55]. In our numerical simulations, we will present examples with kappa set to $\kappa = \frac{4}{\sqrt{2}}$. In this case the superconductor remains type II, but the absence of significantly different length scales simplifies numerical simulations.

Notice that these redefinitions imply that Γ_2 has dimensions of $[L]^2$, while the rest of the parameters are dimensionless. The nematic coherence length with these new variables is calculated as $l_\eta^2 = \frac{\Gamma_2}{\Gamma_4}$.

We will work under the assumption that both superconducting and nematic symmetries are broken. For constant order parameters, the minimum energy is achieved when the interaction potential is minimized,

$$\begin{aligned} V(|\tilde{\psi}|^2, \tilde{\eta}) &= \rho_0 |\alpha_{\text{GL}}| \int_V \frac{1}{2} (|\tilde{\psi}|^2 - 1)^2 \\ &+ \frac{\Gamma_4}{2} (\tilde{\eta}^2 - 1)^2 + \hat{\lambda}_2 |\tilde{\psi}|^2 \tilde{\eta}^2. \quad (15) \end{aligned}$$

On the minimum, the order parameters take the values

$$\tilde{\psi}_v^2 = \frac{1 - \hat{\lambda}_2}{1 - \frac{\hat{\lambda}_2}{\Gamma_4}}, \quad \tilde{\eta}_v^2 = \frac{1 - \frac{\hat{\lambda}_2}{\Gamma_4}}{1 - \frac{\hat{\lambda}_2}{\Gamma_4}}, \quad (16)$$

and thus the free energy is

$$F_0 = |\alpha_{\text{GL}}| \rho_0 V \frac{(\tilde{\psi}_v^2 - 1)(\tilde{\psi}_v^2 + \tilde{\eta}_v^2)}{2\tilde{\eta}_v^2}. \quad (17)$$

For further convenience, we will refer the energy to this value,

$$\tilde{F} = F - F_0. \quad (18)$$

The theory can be reformulated in terms of a dimensionless time parameter τ , related to the physical time t by

$$t = \frac{\hbar^2}{2mD|\alpha_{\text{GL}}|} \tau, \quad (19)$$

if we also redefine the conductivity and the nematic diffusion constant as

$$\sigma_1 = \frac{4\pi\sigma}{c^2} \frac{2mD|\alpha_{\text{GL}}|}{\hbar^2}, \quad D_\eta = D_n(\rho_0/\eta_0^2). \quad (20)$$

The explicit form of the equations can be found in [53].

III. VORTEX-DOMAIN WALL INTERACTION

A. Numerical method

Calculations were performed using the geophysical high-order suite for turbulence (or GHOST for short [56,57]), which uses a high-order pseudospectral method. Following Ref. [58], we consider configurations in a $[0, 2\pi] \times [0, 2\pi]$ simulation box using 512×512 grid points. We only focus on a $[0, \pi] \times [0, \pi]$ sector, since the other sectors serve as images to satisfy the periodicity in the $[0, 2\pi] \times [0, 2\pi]$ domain required by the pseudospectral method. The initial conditions depend on the number of singularities (domain walls or superconducting vortices) under consideration.

As discussed in [53], the initial condition for a single vortex located at $(x/L, y/L) = (\pi/2, \pi/2)$ is taken as

$$\tilde{\psi}(x, y, t = 0) = \tilde{\psi}_v \frac{(\lambda + i\mu)}{\sqrt{\lambda^2 + \mu^2}} \tanh \frac{\sqrt{\lambda^2 + \mu^2}}{\sqrt{2}\xi}, \quad (21)$$

where the Clebsch potentials are $\lambda(x) = \sqrt{2} \cos x$ and $\mu(y) = \sqrt{2} \cos y$ (a shift in the vortex position is trivially achieved by modifying the Clebsch potentials), and the initial condition for the vector potential is

$$a_x(x, y, t = 0) = a_0 \sin(x) \cos(y), \quad (22)$$

$$a_y(x, y, t = 0) = -a_0 \cos(x) \sin(y), \quad (23)$$

which is a well-known initial condition in fluid dynamics known as a Taylor-Green flow. The resulting initial magnetic field $B_z(x, y, t = 0) = 2a_0 \sin x \sin y$ (with a_0 a normalization constant related to the total flux in the simulation box; see [53]) satisfies the necessary conditions of periodicity and is easy to implement numerically.

The positive definiteness of the energy [Eq. (12)] imposes bounds on the parameters of the model; the requirement of working in the phase where both nematicity and superconductivity are active introduces additional constraints. We have provided a detailed discussion of these bounds in Ref. [53]. Furthermore, certain parameter choices have been made for numerical reasons without loss of generality. To prevent unnecessary numerical complications, we have aligned all length and time scales to be of a similar order. It is worth noting

that this last condition could be relaxed for a quantitative comparison with more realistic situations.

For the simulations carried out in this paper, we set the nematic coherence length to be equal to the superconducting coherence length $l_\eta = \xi = 0.04$. As we have mentioned before, the GL parameter will be set as $\kappa = \frac{4}{\sqrt{2}}$. This choice might not be realistic for real superconductors, but makes simulations simpler as all relevant length scales are of the same order. For simplicity, we have also set $\rho_0 = \eta_0 = 1$ and $\Gamma_4 = 1$ (notice that this choice also sets the value of Γ_2). On the other hand, we have chosen $D_n = D = \frac{\hbar}{2m}$, and the dimensionless conductivity as $\sigma_1 = 15$. The values of these constants can be relevant in setting time scales for equilibration processes and energy dissipation but will not alter the main conclusions of this work. An integration time step $dt = 6 \times 10^{-5}$ was used, consistent with the required Courant-Friedrichs-Lewy condition for stability of the numerical solution (see [53]).

B. The superconductor order parameter and the domain wall

It is well known that an Ising-type order parameter theory admits nontrivial solutions representing a two-dimensional defect, or a *domain wall*. For instance, it is easy to check that when $\hat{\lambda}_1 = \hat{\lambda}_2 = 0$, a static solution for $\tilde{\eta}$ is

$$\tilde{\eta}(x) = \tilde{\eta}_v \tanh\left(\frac{x}{\sqrt{2}l_\eta}\right), \quad (24)$$

which represents a domain wall located at $x = 0$, following the typical orientation of a structural twin boundary (the position and orientation of the wall can be easily changed). Here, l_η is the nematic coherence length defined in Eq. (9) and related to the domain wall thickness.

In this subsection, we explore the interaction of a domain wall of this type with a superconducting vortex, placed at different distances from the nematic domain wall. In order to induce the domain wall formation at the $x/L = \pi/2$ plane, we take the initial condition corresponding to the nematic order parameter as

$$\tilde{\eta}(x, y, t = 0) = \frac{\tilde{\eta}_v}{\tanh\left(\frac{1}{\sqrt{2}l_\eta}\right)} \tanh\left(\frac{\lambda(x)}{2l_\eta}\right). \quad (25)$$

As a first test of the numerical method, we verified that for the pure nematic theory, the initial condition (25) evolves to the exact solution (24). The energy per area of the domain wall can be calculated explicitly, resulting in

$$E_{\text{wall}} = \frac{4}{3}\rho_0|\alpha_{\text{GL}}|\sqrt{2\Gamma_2\Gamma_4}, \quad (26)$$

where the area of the wall is $L_y \times L_z = \pi^2$. Our simulations indicate that the initial condition proposed for the nematic order parameter rapidly converges to the exact solution for the wall, and the energy can be numerically computed with precision down to $O(10^{-4})$.

We continue studying the behavior of the superconductor order parameter in the presence of a domain wall. We first consider the case in which $\lambda_2 \neq 0$, $\lambda_1 = 0$, and the initial configuration for the superconductor order parameter is $|\tilde{\psi}|^2 = \rho_0$ (i.e., there is no vortex). We show in Fig. 1(b) [Fig. 1(c)] that superconductivity is enhanced (depressed) for positive

(negative) values of $\hat{\lambda}_2$. This is consistent with the fact that the order parameters compete (cooperate) for positive (negative) values of λ_2 .

C. A single vortex in the presence of a nematic domain wall

We now turn to study the case of a single vortex in the presence of a nematic domain wall. We first study the effect of the biquadratic coupling, and after that we see how these results are modified when the trilinear coupling is active. As we mentioned before, the biquadratic coupling would be present even in cases in which the order parameter was a scalar, so results in this subsection could apply to a more general range of theories.

1. Biquadratic coupling

Before entering into the details of the simulations, it is clear that for $\lambda_2 > 0$ ($\lambda_2 < 0$) the interaction will be repulsive (attractive). Because superconductivity is enhanced for positive coupling, the vortex will move its normal core away from the wall in order to minimize the free energy, thus exhibiting a repulsive interaction between the vortex and the domain wall. On the other hand, since superconductivity is depressed for negative coupling, we expect that the normal core will tend to remain on the domain wall, resulting instead in an attractive interaction. It is also easy to predict that the interaction is short-ranged.

We show in the top panel of Fig. 2 the density plot of $|\tilde{\psi}(x, y)|^2$ for the attractive case ($\lambda_2 < 0$). We start with a vortex at a distance $d = 3\xi$ from the domain wall, and after a finite time the vortex becomes pinned to the wall. Notice that the wall has its own dynamics, and it bends during the pinning process. The rigidity of the wall is controlled by the parameters of the theory. In the bottom panel of Fig. 2 we show the same density plot but for the repulsive case ($\lambda_2 > 0$). For this simulation, we placed the vortex within the domain wall and waited until it was repelled. Remember that the effective superconducting coherence length depends on the value and sign of λ_2 , and thus the core size is noticeably larger than in the attractive case. The wall bending effect is also more pronounced in the repulsive than in the attractive case.

Far from the domain wall the vortex core has cylindrical symmetry, but as it is attracted to the NDW the vortex loses this symmetry and ends up elongated along the direction selected by the domain wall. The lack of cylindrical symmetry is more evident when the λ_1 coupling is turned on, as we will discuss soon. Since there is no direct coupling between the vector potential and the nematic order parameter, the lack of cylindrical symmetry is less pronounced in the magnetic field (not shown).

We now characterize the interaction between the vortex and the domain wall in a more quantitative way. For the sake of clarity, we mostly focus on the repulsive case (a similar analysis can be performed for the attractive case). In Fig. 3 we show the trajectory of the vortex core as a function of time, the interaction energy per unit length, and the force per unit length as a function of the distance of the vortex core to the wall, for different values of the biquadratic coupling parameter. For these simulations, the vortex was placed on top of the domain wall in an unstable equilibrium, signed by the transient time

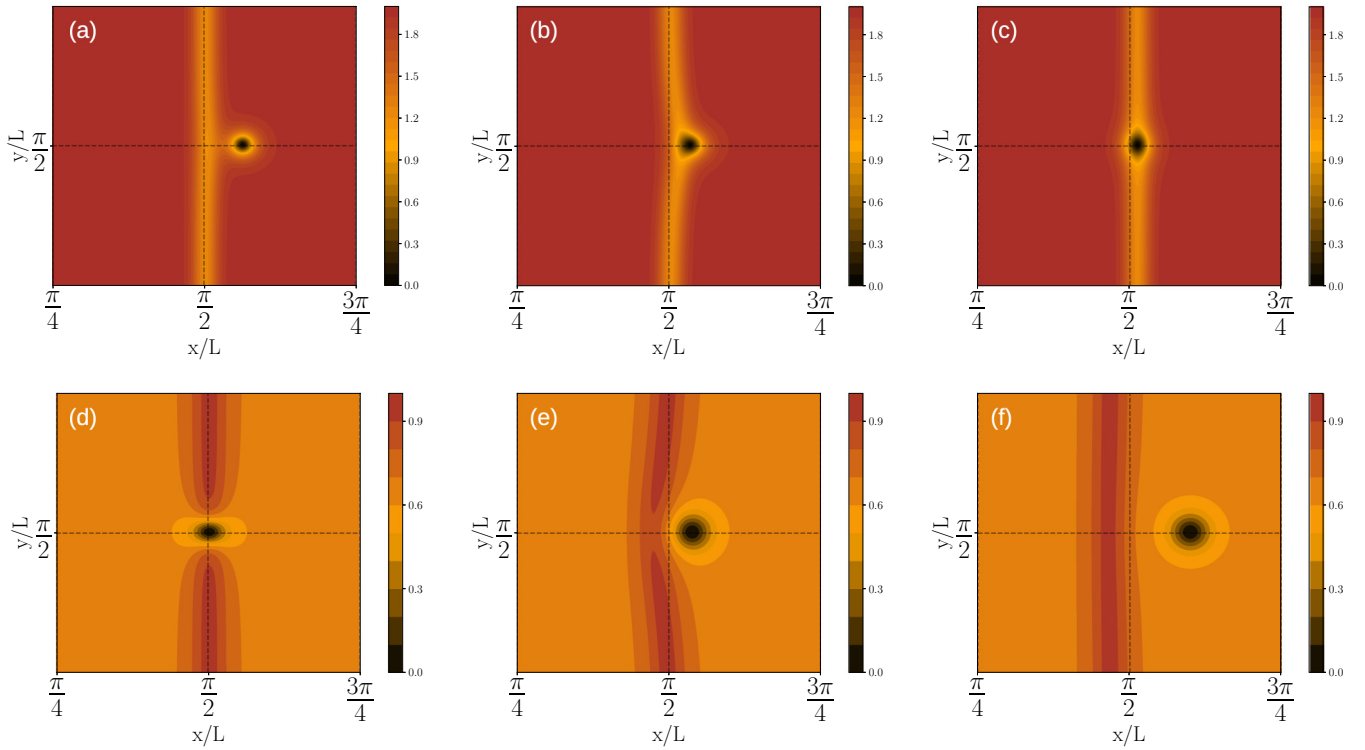


FIG. 2. (a)–(c) Snapshots of the density plot of $|\tilde{\psi}|^2$ for the purely biquadratic case in the attractive regime with $\hat{\lambda}_2 = -0.5$ and a wall width of $l_\eta = \xi = 0.04$. The vertical (horizontal) dashed line represents the $x = \pi/2$ ($y = \pi/2$) axis, for visual guidance. Once the vortex is pinned, it changes its symmetry to align with the direction selected by the wall. (d)–(f) Same plots as (a)–(c) but for the repulsive case with $\hat{\lambda}_2 = 0.5$ and the same wall width. The domain wall bends sharply as the vortex is repelled and retakes its original form once the vortex is far from the wall. Notice that once the vortex leaves the domain wall, it retains its cylindrical symmetry (see the text below).

that it takes for the vortex to begin its movement. We see that the vortex acquires maximum acceleration at the boundary of the wall, as shown in Fig. 3(a).

To calculate the interaction energy, we first calculate the domain wall energy and the energy of an isolated vortex (with no domain wall), and we then subtract these energies from the total energy in the simulation domain. More precisely, we are interested in energies per unit length of the vortex. As we

are assuming translational symmetry along the c axes, this amounts to integrating over the ab plane. Notice that we defined dimensionless coordinates $\tilde{x} = x/\xi$, $\tilde{y} = y/\xi$, and field $\tilde{\mathbf{a}} = \mathbf{a}/\xi$. Thus, energies per unit length can be expressed as

$$\tilde{E} = \tilde{E}_0 \mathcal{E}, \quad (27)$$

where \mathcal{E} is a dimensionless function of the variables κ , $\hat{\lambda}_1$, $\hat{\lambda}_2$, Γ_4 , and Γ_2/ξ^2 , and \tilde{E}_0 sets the scale for the energy per

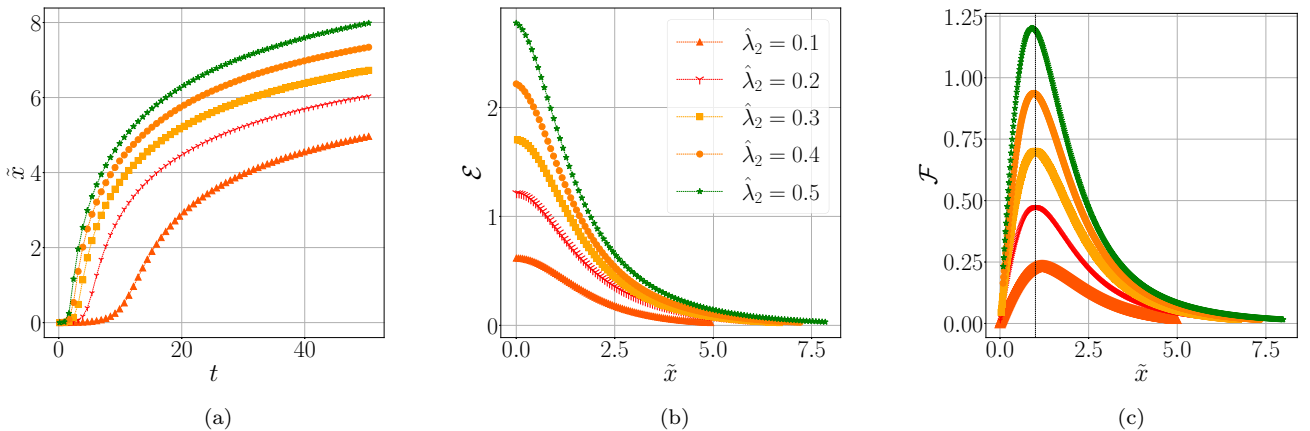


FIG. 3. (a) Distance of the vortex from the NDW, measured from the center of the wall, as a function of time for different values of $\hat{\lambda}_2$ (with $\hat{\lambda}_1 = 0$). (b) Dimensionless interaction energy as a function of the distance of the vortex to the center of the NDW [see Eqs. (27)–(30) for definitions]. (c) Dimensionless interaction force as a function of the vortex distance from the NDW. The dashed vertical line indicates the domain wall edge.

TABLE I. Fitting parameters for the energy as a function of the vortex–domain wall distance in the biquadratic repulsive regime (see text for details).

$\hat{\lambda}_2$	\mathcal{E}_0	c_1	c_2
0.1	0.617	1.658	2.434
0.2	1.176	2.490	2.757
0.3	1.703	3.358	3.044
0.4	2.223	4.546	3.413
0.5	2.761	6.328	3.922

unit length,

$$\tilde{E}_0 = |\alpha_{\text{GL}}| \rho_0 \xi^2 = \frac{|\alpha_{\text{GL}}|^2}{\beta} \xi^2 = \frac{H_c^2}{4\pi} \xi^2, \quad (28)$$

where H_c is the thermodynamic superconducting critical magnetic field.

We can define the dimensionless interaction energy between the vortex and the NDW as

$$\mathcal{E}_{\text{int}} = \frac{\tilde{E}_T - \tilde{E}_{\text{vortex}} - \tilde{E}_{\text{wall}}}{\tilde{E}_0}. \quad (29)$$

Using these data, we can reconstruct $\mathcal{E}_{\text{int}}(x)$ and calculate the effective force per unit length \tilde{F}_{eff} between the vortex and the wall as

$$\tilde{F}_{\text{eff}} = -\frac{\partial \mathcal{E}_{\text{int}}}{\partial x} = F_0 \mathcal{F} = \frac{H_c^2}{4\pi} \xi \mathcal{F}, \quad (30)$$

where \mathcal{F} is a dimensionless function. The data can be fitted by a simple expression of the type

$$\mathcal{E}_{\text{fit}} = \frac{\mathcal{E}_0}{1 + c_1 \sinh^2 \frac{x}{c_2}}. \quad (31)$$

The coefficients that fit the aforementioned energies can be found in Table I.

Figure 3(c) shows the calculated interaction force between the domain wall and the vortex, where we have scaled the position in units of the coherence length. Notice that the maximum of the force occurs in the vicinity of the domain wall edge, marked by the dashed vertical line in Fig. 3(c). The

force exponentially tends to zero as the vortex leaves the wall, confirming the short-range nature of the interaction.

2. The effect of the trilinear term

We next study the case in which the C_4 breaking coupling is present. It has been observed in many experiments (see below) that vortices are elliptical with the axes of the ellipsoid oriented along the axes of the orthorhombic phase. The trilinear term in our model reproduces that effect. To see this, we take the trilinear term with η constant and fixed. Then, the free energy is

$$\tilde{F}_s = \int_V \tilde{\alpha}_{\text{GL}} |\psi|^2 + \frac{\beta}{2} |\psi|^4 + \frac{\hbar^2}{2m} l_{ij} \mathcal{D}_i \psi \mathcal{D}_j \psi^* + \frac{(\nabla \times \mathbf{A})^2}{8\pi},$$

where $\tilde{\alpha}_{\text{GL}} = \alpha_{\text{GL}} + \lambda_2 \eta^2$ and

$$l_{ij} = \delta_{ij} + \lambda_1 e_{ij} = (1 - \lambda_1 \eta) \delta_{ij} + 2\lambda_1 \eta n_i n_j. \quad (32)$$

After using the expression of n_i with $\alpha = \pi/4$, this becomes

$$\mathbf{l} = \mathbf{I}_{2 \times 2} + \lambda_1 \eta \sigma_1, \quad (33)$$

with σ_1 the symmetric Pauli matrix. The eigenvalues of \mathbf{l} are

$$l_{\pm} = 1 \pm |\lambda_1 \eta|, \quad (34)$$

resulting in elliptical vortices with core size axes

$$\xi_{\pm}^2 = \frac{\hbar^2 l_{\pm}}{2m\tilde{\alpha}_{\text{GL}}}. \quad (35)$$

Defining the eccentricity of an ellipse as $e = (1 - a_-^2/a_+^2)^{1/2}$, where a_+ (a_-) are the larger and smaller axes, we obtain that $e = [2|\lambda_1 \eta|/(1 + |\lambda_1 \eta|)]^{1/2}$ (remember that within our approach $|\lambda_1 \eta| < 1$, and hence $e < 1$).

We next consider the dynamics of an elliptical vortex in the presence of a domain wall. The description in this case is not intuitive as we find the opposite behavior to that observed before for $\lambda_1 = 0$: the trajectory of the vortex is not a straight line perpendicular to the wall. In Fig. 4 we present snapshots of the superconductor order parameter for $\lambda_2 = 0.5$ and $\lambda_1 = 0.5$. As before, we have chosen for this figure the bare nematic coherence length to be $l_\eta = \xi$. A positive $\hat{\lambda}_2$

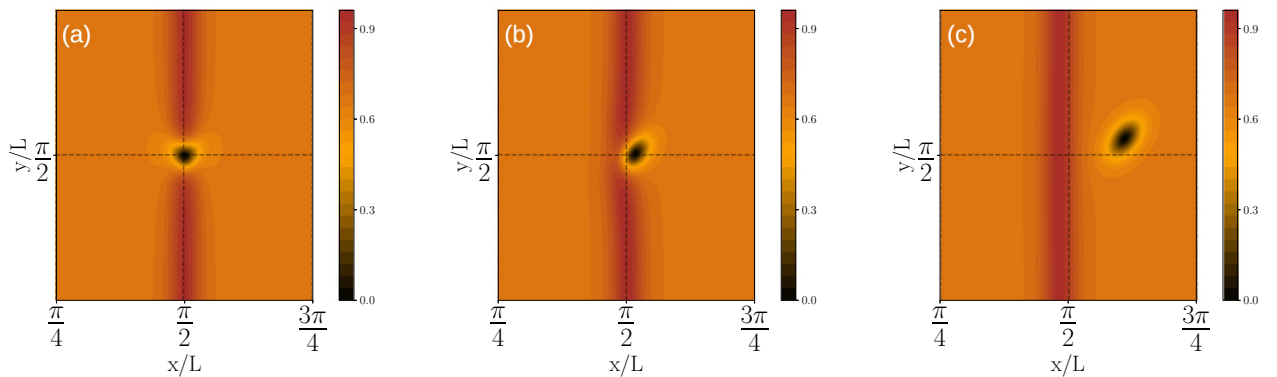


FIG. 4. Snapshots of the superconductor order parameter $|\tilde{\psi}|^2$ with C_4 symmetry-breaking coupling $\hat{\lambda}_1 = 0.5$ and a repulsive interaction with the wall $\hat{\lambda}_2 = 0.5$. The GL parameter is set as $\kappa = \frac{4}{\sqrt{2}}$. The wall width is the same as the superconductor coherence length. As the vortex leaves the wall, the trajectory deviates from the $y = \pi/2$ line, as opposed to the purely biquadratic coupling, where the trajectory evolves along curves with constant y .

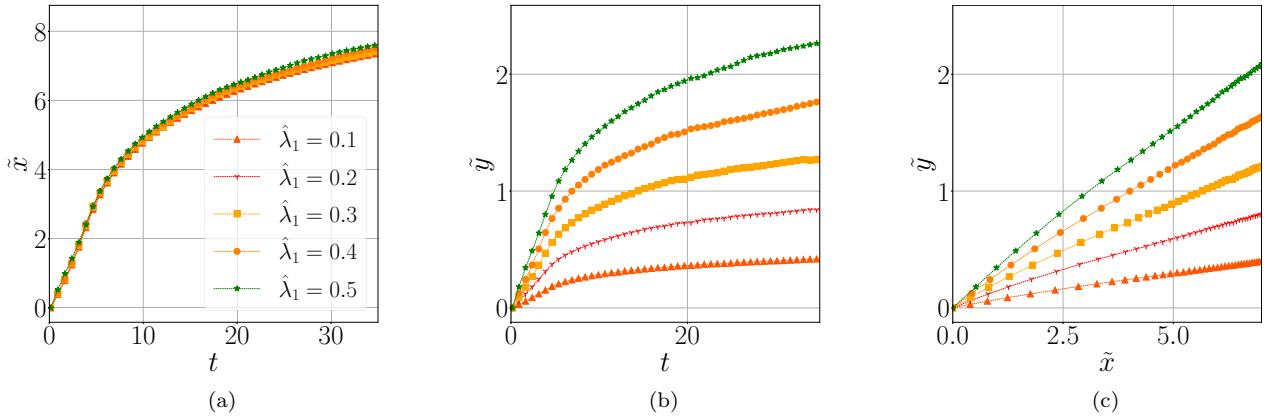


FIG. 5. Panels (a) and (b) show $\tilde{x}(t)$ and $\tilde{y}(t)$, respectively, measured from the center of the NDW, as a function of time for different values of $\hat{\lambda}_1$. (c) Vortex trajectories $\tilde{y}(\tilde{x}(t))$ for several values of $\hat{\lambda}_1$. As the coupling tends to zero, the trajectory becomes perpendicular to the NDW.

causes the vortex to be repelled perpendicular to the wall into a region of increasing nematic order parameter, where the vortex becomes more elliptical as the nematicity increases, as $\hat{\lambda}_1 = 0.5$. This causes the vortex to deviate from its expected perpendicular trajectory.

In Fig. 5 we show the coordinates $\tilde{x}(t)$, $\tilde{y}(t)$ of the vortex as a function of time, and the trajectories in the plane $\tilde{y}(\tilde{x})$ for fixed $\hat{\lambda}_2$ and varying $\hat{\lambda}_1$. Contrary to the purely biquadratic case, the vortex trajectory has a component parallel to the wall. While the component perpendicular to the wall is weakly affected by the value of $\hat{\lambda}_1$ [see Fig. 5(a)], the component parallel to the wall [see Fig. 5(b)] is roughly linear with $\hat{\lambda}_1$. Plotting the trajectories followed by the vortices [Fig. 5(c)] we notice that deviation angles are directly proportional to $\hat{\lambda}_1$ and, as expected, the angle tends to zero when $\lambda_1 \rightarrow 0$.

For the attractive case, the vortex is pinned to the wall. Due to the different values of the nematic order parameter

across the wall, the vortex core displays a peculiar symmetry pattern corresponding to the superposition of two ellipses with axes that are rotated at different sides of the wall, producing a structure with a heart-shaped core. Indeed, as shown in Fig. 6(a), the vortex core is well described by the contour lines of the “heart” function,

$$h(x, y) = (x - x_0)^2 + (y - y_0)^2 \pm 2|\lambda_1 \eta_v| |x - x_0|(y - y_0), \quad (36)$$

where $(x_0, y_0) = (\pi/2, \pi/2)$ corresponds to the center of the vortex. This pattern for a vortex core pinned to a wall is indeed very similar to the one observed via STM measurements for FeSe in Ref. [44]. Note that even though the GL theory considered here is simpler than the one used in Ref. [44], the pinned vortex shape is very similar to that found in theoretical and experimental studies.

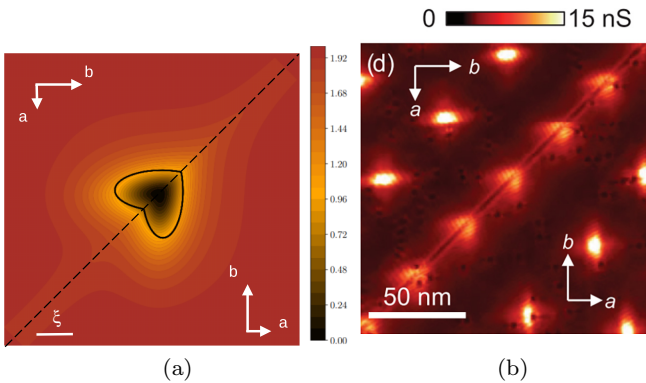


FIG. 6. (a) Calculated density of the superconductor order parameter $|\tilde{\psi}|^2$ for a vortex pinned to a nematic domain wall with $\hat{\lambda}_1 = 0.5$ and $\kappa = \frac{4}{\sqrt{2}}$. The nematic domain wall is represented by the black dotted line, and the orthorhombic a and b axes on each domain are shown with white arrows. (b) Experimental zero-bias conductance image from Watashige *et al.* [44], showing vortices pinned to a domain wall at $T = 1.5$ K and a magnetic field of 1 T applied along the c axis. Crystallographic axes are shown by white arrows. Note that the color code between figures in both panels is inverted: in panel (a) dark corresponds to the vortex core, while in (b) the core is represented with white.

IV. SUMMARY AND CONCLUSIONS

In this paper, we addressed vortex-nematic domain wall interactions in a Ginzburg-Landau theory of an s -wave superconductor interacting with a real (Ising-type) nematic order parameter. The choice of a real order parameter (as opposed to nematic order in liquids described by a tensor order parameter) is inspired by the phenomenology of Fe-based superconductors, where nematicity manifests as the breaking of a C_4 symmetry down to a C_2 symmetry. Since the nematic order parameter is of Ising-type, it gives rise to domains whose presence is eventually dictated by boundary conditions, thermal history, and additional interactions of the nematic order parameter with other degrees of freedom.

In the simple GL theory, we have considered the superconductor order parameter, and the nematic order parameter interaction is introduced via two terms: a biquadratic coupling and a trilinear derivative coupling. The biquadratic term is mainly responsible for the attractive or repulsive character of the interaction, while the trilinear term modifies the in-plane superconductivity, affecting the shape of the vortex and its trajectory (that is not necessarily a straight line perpendicular to the wall in the repulsive case).

In Fe-based superconductors, the nematic domain walls are often linked to twin boundaries separating two different orthorhombic domains. A more complete treatment of the problem would then require the introduction of elastic terms in the free energy, taking into account the coupling of these elastic terms with the superconductor order parameters and the nematic order parameter. For symmetry reasons, it is expected that twin-boundaries and nematic walls will be strongly coupled. In the simplest scenario, it is usually assumed that they are superimposed. Yet their properties could be different. For instance, their width, and as a consequence the extent of its influence on the superconducting properties, could differ. Thus, the final behavior of the vortex will be the result of these two combined effects, i.e., vortex-nematic domain wall and vortex-twin boundary interaction.

Despite its simplicity, the model captures some relevant features of vortices in Fe-based superconductors. As an example, the elongated vortex shape, related in our calculations to the trilinear derivative coupling, has been observed in FeSe crystalline films (see, e.g. [42]). The attractive vortex-domain wall interaction that results in our model mainly from a negative bi-quadratic coupling term is consistent with the observed vortex accumulation on FeSe domain boundaries, where degraded superconductivity was found [42,44]. On the other hand, the repulsive character observed in underdoped $\text{Ba}(\text{Fe}_{1-x}\text{Co}_x)_2\text{As}_2$, explained by the observation of enhanced superfluid density on twin boundaries [33], is consistent with a positive bi-quadratic coupling term. As for the calculated peculiar cordate vortex core shape formed when the vortex is pinned on a domain wall, as shown in Fig. 6(a), it is remarkably similar to the shape observed by the STM measurements shown in Fig. 6(b) for cleaved single FeSe crystals [44]. Furthermore, there are some interesting features predicted by the model still to be explored experimentally through direct observation techniques in Fe-based compounds, such as the relationship between the anisotropy of the vortex core, domain wall directions, and vortex trajectories.

Finally, there are several lines of research in which our research can be extended. As mentioned before, the introduction in the formalism of the elastic degrees of freedom is fundamental to understanding the resulting NDM/TB interaction. Thermal effects in the Ginzburg-Landau framework are typically introduced through the temperature dependence of parameters, notably the quadratic terms in the potential. Alternatively, they can be incorporated by introducing thermal noise to the time-dependent Ginzburg-Landau equations, with correlations that are temperature-dependent. From a theoretical standpoint, there is no requirement for the two transitions to occur simultaneously. In fact, scenarios of non-symmetry-restoration have been discussed in other situations, especially in cases involving a negative value for the biquadratic term [59]. For realistic Fe-based samples, the nematic transition normally occurs at a higher temperature than the superconducting one and the transition temperatures are doping-dependent. The inclusion of thermal effects in the TDGL approach for nematic superconductors is undoubtedly an interesting point that we plan to explore in the future. Finally, the implementation of appropriate boundary conditions to describe vortex lattices, and the way lattices are affected by the presence of domains and the introduction of external currents to study the dynamics of pinning, are of interest. We hope to return to these questions in future studies.

ACKNOWLEDGMENTS

R.S.S., V.B., G.P., and G.S.L. acknowledge support by Universidad de Buenos Aires, Grant No. UBA-CyT 20020170100496BA, by ANPCYT, Grant No. PICT Raices 2019-015890, and by CONICET, Grant No. PIP 11220150100653CO. P.D.M. acknowledges financial support from Universidad de Buenos Aires, Grant No. UBACYT 20020170100508BA, and by ANPCYT, Grant No. PICT 2018-4298. E.F. acknowledges support by the U.S. National Science Foundation under Grant DMR-2225920 at the University of Illinois.

-
- [1] S. A. Kivelson, E. Fradkin, and V. J. Emery, Electronic liquid-crystal phases of a doped mott insulator, *Nature (London)* **393**, 550 (1998).
 - [2] E. Fradkin, S. A. Kivelson, M. J. Lawler, J. P. Eisenstein, and A. P. Mackenzie, Nematic fermi fluids in condensed matter physics, *Annu. Rev. Condens. Matter Phys.* **1**, 153 (2010).
 - [3] M. P. Lilly, K. B. Cooper, J. P. Eisenstein, L. N. Pfeiffer, and K. W. West, Evidence for an anisotropic state of two-dimensional electrons in high landau levels, *Phys. Rev. Lett.* **82**, 394 (1999).
 - [4] E. Fradkin and S. A. Kivelson, Liquid-crystal phases of quantum hall systems, *Phys. Rev. B* **59**, 8065 (1999).
 - [5] R. A. Borzi, S. A. Grigera, J. Farrell, R. S. Perry, S. J. S. Lister, S. L. Lee, D. A. Tennant, Y. Maeno, and A. P. Mackenzie, Formation of a Nematic Fluid at High Fields in $\text{Sr}_3\text{Ru}_2\text{O}_7$, *Science* **315**, 214 (2007).
 - [6] E. Fradkin, S. A. Kivelson, and J. M. Tranquada, Colloquium: Theory of intertwined orders in high temperature superconductors, *Rev. Mod. Phys.* **87**, 457 (2015).
 - [7] R. F. Fernandes, A. I. Coldea, H. Ding, I. R. Fisher, P. J. Hirschfeld, and G. Kotliar, Iron pnictides and chalcogenides: a new paradigm for superconductivity, *Nature (London)* **601**, 35 (2022).
 - [8] Y. Ando, K. Segawa, S. Komiyama, and A. N. Lavrov, Electrical resistivity anisotropy from self-organized one dimensionality in high-temperature superconductors, *Phys. Rev. Lett.* **88**, 137005 (2002).
 - [9] V. Hinkov, D. Haug, B. Fauqué, P. Bourges, Y. Sidis, A. Ivanov, C. Bernhard, C. T. Lin, and B. Keimer, Electronic liquid crystal state in the high-temperature superconductor $\text{YBa}_2\text{Cu}_3\text{O}_{6.45}$, *Science* **319**, 597 (2008).
 - [10] R. Comin, R. Sutarto, E. H. da Silva Neto, L. Chauviere, R. Liang, W. N. Hardy, D. A. Bonn, F. He, G. A. Sawatzky, and A. Damascelli, Broken translational and rotational symmetry via charge stripe order in underdoped $\text{YBa}_2\text{Cu}_3\text{O}_{6+y}$, *Science* **347**, 1335 (2015).
 - [11] T.-M. Chuang, M. P. Allan, J. Lee, Y. Xie, N. Ni, S. L. Bud'ko, G. S. Boebinger, P. C. Canfield, and J. C. Davis, Nematic

- electronic structure in the “parent” state of the iron-based superconductor $\text{Ca}(\text{Fe}_{1-x}\text{Co}_x)_2\text{As}_2$, *Science* **327**, 181 (2010).
- [12] R. Prozorov, M. A. Tanatar, N. Ni, A. Kreyssig, S. Nandi, S. L. Bud’ko, A. I. Goldman, and P. C. Canfield, Intrinsic pinning on structural domains in underdoped single crystals of $\text{Ba}(\text{Fe}_{1-x}\text{Co}_x)_2\text{As}_2$, *Phys. Rev. B* **80**, 174517 (2009).
- [13] H. Kuo, J. Chu, J. C. Palmstrom, S. A. Kivelson, and I. R. Fisher, Ubiquitous signatures of nematic quantum criticality in optimally doped Fe-based superconductors, *Science* **352**, 958 (2016).
- [14] J.-H. Chu, J. G. Analytis, K. De Greve, P. L. McMahon, Z. Islam, Y. Yamamoto, and I. R. Fisher, In-plane resistivity anisotropy in an underdoped iron arsenide superconductor, *Science* **329**, 824 (2010).
- [15] H. H. Kuo, J. G. Analytis, J. H. Chu, R. M. Fernandes, J. Schmalian, and I. R. Fisher, Magnetoelastically coupled structural, magnetic, and superconducting order parameters in $\text{BaFe}_2(\text{As}_{1-x}\text{P}_x)_2$, *Phys. Rev. B* **86**, 134507 (2012).
- [16] Y. Gallais, R. M. Fernandes, I. Paul, L. Chauvière, Y.-X. Yang, M.-A. Méasson, M. Cazayous, A. Sacuto, D. Colson, and A. Forget, Observation of incipient charge nematicity in $\text{Ba}(\text{Fe}_{1-x}\text{Co}_x)_2\text{As}_2$, *Phys. Rev. Lett.* **111**, 267001 (2013).
- [17] M. A. Tanatar, A. E. Böhmer, E. I. Timmons, M. Schütt, G. Drachuck, V. Taufour, K. Kothapalli, A. Kreyssig, S. L. Bud’ko, P. C. Canfield, R. M. Fernandes, and R. Prozorov, Origin of the resistivity anisotropy in the nematic phase of FeSe, *Phys. Rev. Lett.* **117**, 127001 (2016).
- [18] F. Kretzschmar, T. Böhm, U. Karahasanovic, B. Muschler, A. Baum, D. Jost, J. Schmalian, S. Caprara, M. Grilli, C. Di Castro, J. G. Analytis, J.-H. Chu, I. R. Fisher, and R. Hackl, Critical spin fluctuations and the origin of nematic order in $\text{Ba}(\text{Fe}_{1-x}\text{Co}_x)_2\text{As}_2$, *Nat. Phys.* **12**, 560 (2016).
- [19] C. Eckberg, D. J. Campbell, T. Metz, J. Collini, H. Hodovanets, T. Drye, P. Zavalij, M. H. Christensen, R. M. Fernandes, S. Lee, P. Abbamonte, J. W. Lynn, and J. Paglione, Sixfold enhancement of superconductivity in a tunable electronic nematic system, *Nat. Phys.* **16**, 346 (2020).
- [20] S. Lee, J. Collini, S. X.-L. Sun, M. Mitrano, X. Guo, C. Eckberg, J. Paglione, E. Fradkin, and P. Abbamonte, Multiple charge density waves and superconductivity nucleation at antiphase domain walls in the nematic pnictide $\text{Ba}_{1-x}\text{Sr}_x\text{Ni}_2\text{As}_2$, *Phys. Rev. Lett.* **127**, 027602 (2021).
- [21] S. Manzeli, D. Ovchinnikov, D. Pasquier, O. V. Yazyev, and A. Kis, 2d transition metal dichalcogenides, *Nat. Rev. Mater.* **2**, 17033 (2017).
- [22] S. D. Wilson and B. R. Ortiz, AV_3Sb_5 Kagome Superconductors: Progress and future directions, [arXiv:2311.05946](https://arxiv.org/abs/2311.05946).
- [23] V. Oganesyan, S. A. Kivelson, and E. Fradkin, Quantum theory of a nematic fermi fluid, *Phys. Rev. B* **64**, 195109 (2001).
- [24] C. J. Halboth and W. Metzner, d -wave superconductivity and pomeranchuk instability in the two-dimensional hubbard model, *Phys. Rev. Lett.* **85**, 5162 (2000).
- [25] W. Metzner, D. Rohe, and S. Andergassen, Soft fermi surfaces and breakdown of fermi-liquid behavior, *Phys. Rev. Lett.* **91**, 066402 (2003).
- [26] S. A. Kivelson, E. Fradkin, and T. H. Geballe, Quasi-one-dimensional dynamics and nematic phases in the two-dimensional emery model, *Phys. Rev. B* **69**, 144505 (2004).
- [27] W. Lv, J. Wu, and P. Phillips, Orbital ordering induces structural phase transition and the resistivity anomaly in iron pnictides, *Phys. Rev. B* **80**, 224506 (2009).
- [28] C. Xu, M. Müller, and S. Sachdev, Ising and spin orders in the iron-based superconductors, *Phys. Rev. B* **78**, 020501(R) (2008).
- [29] C. Fang, H. Yao, W.-F. Tsai, J. P. Hu, and S. A. Kivelson, Theory of electron nematic order in lafeaso, *Phys. Rev. B* **77**, 224509 (2008).
- [30] L. Nie, A. V. Maharaj, E. Fradkin, and S. A. Kivelson, Vestigial nematicity from spin and/or charge order in the cuprates, *Phys. Rev. B* **96**, 085142 (2017).
- [31] R. M. Fernandes, P. P. Orth, and J. Schmalian, Intertwined vestigial order in quantum materials: Nematicity and beyond, *Annu. Rev. Condens. Matter Phys.* **10**, 133 (2019).
- [32] J.-H. Chu, H.-H. Kuo, J. G. Analytis, and I. R. Fisher, Divergent nematic susceptibility in an iron arsenide superconductor, *Science* **337**, 710 (2012).
- [33] B. Kalisky, J. R. Kirtley, J. G. Analytis, J.-H. Chu, A. Vailionis, I. R. Fisher, and K. A. Moler, Stripes of increased diamagnetic susceptibility in underdoped superconducting $\text{Ba}(\text{Fe}_{1-x}\text{Co}_x)_2\text{As}_2$ single crystals: Evidence for an enhanced superfluid density at twin boundaries, *Phys. Rev. B* **81**, 184513 (2010).
- [34] J. J. Sanchez, P. Malinowski, J. Mutch, J. Liu, J. W. Kim, P. J. Ryan, and J. Chu, The transport-structural correspondence across the nematic phase transition probed by elasto x-ray diffraction, *Nat. Mater.* **20**, 1519 (2021).
- [35] J. M. Bartlett, A. Steppke, S. Hosoi, H. Noad, J. Park, C. Timm, T. Shibauchi, A. P. Mackenzie, and C. W. Hicks, Relationship between transport anisotropy and nematicity in FeSe, *Phys. Rev. X* **11**, 021038 (2021).
- [36] G. Blatter, M. V. Feigel’man, V. B. Geshkenbein, A. I. Larkin, and V. M. Vinokur, Vortices in high-temperature superconductors, *Rev. Mod. Phys.* **66**, 1125 (1994).
- [37] W. K. Kwok, J. A. Fendrich, V. M. Vinokur, A. E. Koshelev, and G. W. Crabtree, Vortex shear modulus and lattice melting in twin boundary channels of $\text{YBa}_2\text{Cu}_3\text{O}_{7-\delta}$, *Phys. Rev. Lett.* **76**, 4596 (1996).
- [38] G. W. Crabtree, G. K. Leaf, H. G. Kaper, V. M. Vinokur, A. E. Koshelev, D. W. Braun, D. M. Levine, W. K. Kwok, and J. A. Fendrich, Time-dependent ginzburg-landau simulations of vortex guidance by twin boundaries, *Physica C* **263**, 401 (1996).
- [39] J. A. Herbsommer, G. Nieva, and J. Luzuriaga, Interplay between pinning energy and vortex interaction in $\text{YBa}_2\text{Cu}_3\text{O}_{7-\delta}$ with oriented twin boundaries in tilted magnetic fields: Bitter decoration and tilt-modulus measurements, *Phys. Rev. B* **62**, 3534 (2000).
- [40] M. Marziali Bermúdez, G. Pasquini, S. L. Bud’ko, and P. C. Canfield, Correlated vortex pinning in slightly orthorhombic twinned $\text{Ba}(\text{Fe}_{1-x}\text{Co}_x)_2\text{As}_2$ single crystals: Possible shift of the vortex-glass/liquid transition, *Phys. Rev. B* **87**, 054515 (2013).
- [41] J. Schmidt, V. Bekeris, G. S. Lozano, M. V. Bortule, M. Marziali Bermudez, C. W. Hicks, P. C. Canfield, E. Fradkin, and G. Pasquini, Nematicity in the superconducting mixed state of strain detwinned underdoped $\text{Ba}(\text{Fe}_{1-x}\text{Co}_x)_2\text{As}_2$, *Phys. Rev. B* **99**, 064515 (2019).

- [42] C. L. Song, Y. L. Wang, P. Cheng, Y. P. Jiang, W. Li, T. Zhang, Z. Li, K. He, L. Wang, J. F. Jia *et al.*, Direct observation of nodes and twofold symmetry in fese superconductor, *Science* **332**, 1410 (2011).
- [43] C. L. Song, Y. L. Wang, Y. P. Jiang, L. Wang, K. He, X. Chen, J. E. Hoffman, X. C. Ma, and Q. K. Xue, Suppression of superconductivity by twin boundaries in FeSe, *Phys. Rev. Lett.* **109**, 137004 (2012).
- [44] T. Watashige, Y. Tsutsumi, T. Hanaguri, Y. Kohsaka, S. Kasahara, A. Furusaki, M. Sgrist, C. Meingast, T. Wolf, H. v. Löhneysen, T. Shibauchi, and Y. Matsuda, Evidence for time-reversal symmetry breaking of the superconducting state near twin-boundary interfaces in FeSe revealed by scanning tunneling spectroscopy, *Phys. Rev. X* **5**, 031022 (2015).
- [45] I. P. Zhang *et al.*, Imaging anisotropic vortex dynamics in FeSe, *Phys. Rev. B* **100**, 024514 (2019).
- [46] Y. Yin *et al.*, Scanning tunneling spectroscopy and vortex imaging in the iron pnictide superconductor $\text{BaFe}_{1.8}\text{Co}_{0.2}\text{As}_2$, *Phys. Rev. Lett.* **102**, 097002 (2009).
- [47] B. Kalisky, J. R. Kirtley, J. G. Analytis, J.-H. Chu, I. R. Fisher, and K. A. Moler, Behavior of vortices near twin boundaries in underdoped $\text{Ba}(\text{Fe}_{1-x}\text{Co}_x)_2\text{As}_2$, *Phys. Rev. B* **83**, 064511 (2011).
- [48] A. Yagil, Y. Lamhot, A. Almoalem, S. Kasahara, T. Watashige, T. Shibauchi, Y. Matsuda, and O. M. Auslaender, Diamagnetic vortex barrier stripes in underdoped $\text{BaFe}_2(\text{As}_{1-x}\text{P}_x)_2$, *Phys. Rev. B* **94**, 064510 (2016).
- [49] J. Hecher, S. Ishida, D. Song, H. Ogino, A. Iyo, H. Eisaki, M. Nakajima, D. Kagerbauer, and M. Eisterer, Direct observation of in-plane anisotropy of the superconducting critical current density in $\text{Ba}(\text{Fe}_{1-x}\text{Co}_x)_2\text{As}_2$ crystals, *Phys. Rev. B* **97**, 014511 (2018).
- [50] T. Hashimoto, Y. Ota, H. Q. Yamamoto *et al.*, Superconducting gap anisotropy sensitive to nematic domains in fese, *Nat. Commun.* **9**, 282 (2018).
- [51] Z. Ren *et al.*, Nanoscale decoupling of electronic nematicity and structural anisotropy in fese thin films, *Nat. Commun.* **12**, 10 (2021).
- [52] D. Chowdhury, E. Berg, and S. Sachdev, Nematic order in the vicinity of a vortex in superconducting FeSe, *Phys. Rev. B* **84**, 205113 (2011).
- [53] R. S. Severino, P. D. Mininni, E. Fradkin, V. Bekeris, G. Pasquini, and G. S. Lozano, Vortices in a ginzburg-landau theory of superconductors with nematic order, *Phys. Rev. B* **106**, 094512 (2022).
- [54] A. Schmid, A time dependent Ginzburg-Landau equation and its application to the problem of resistivity in the mixed state, *Phys. Kondens. Mater.* **5**, 302 (1966).
- [55] M. R. Eskildsen, E. M. Forgan, and H. Kawano-Furukawa, Vortex structures, penetration depth and pairing in iron-based superconductors studied by small-angle neutron scattering, *Rep. Prog. Phys.* **74**, 124504 (2011).
- [56] P. D. Mininni, D. Rosenberg, R. Reddy, and A. Pouquet, A hybrid mpi-openmp scheme for scalable parallel pseudospectral computations for fluid turbulence, *Parallel Comput.* **37**, 316 (2011).
- [57] D. Rosenberg, P. D. Mininni, R. Reddy, and A. Pouquet, Gpu parallelization of a hybrid pseudospectral geophysical turbulence framework using cuda, *Atmosphere* **11**, 178 (2020).
- [58] C. Nore, M. Abid, and M. E. Brachet, Decaying kolmogorov turbulence in a model of superflow, *Phys. Fluids* **9**, 2644 (1997).
- [59] G. Bimonte and G. Lozano, Symmetry nonrestoration and inverse symmetry breaking on the lattice, *Phys. Lett. B* **388**, 692 (1996).